



A Journal of the Gesellschaft Deutscher Chemiker

Angewandte Chemie

GDCh

International Edition

www.angewandte.org

Accepted Article

Title: Pre-targeted Imaging of Protease Activity Via In Situ Assembly of Nanoparticles

Authors: Jianghong Rao, Zixin Chen, Min Chen, and Kaixiang Zhou

This manuscript has been accepted after peer review and appears as an Accepted Article online prior to editing, proofing, and formal publication of the final Version of Record (VoR). This work is currently citable by using the Digital Object Identifier (DOI) given below. The VoR will be published online in Early View as soon as possible and may be different to this Accepted Article as a result of editing. Readers should obtain the VoR from the journal website shown below when it is published to ensure accuracy of information. The authors are responsible for the content of this Accepted Article.

To be cited as: *Angew. Chem. Int. Ed.* 10.1002/anie.201916352
Angew. Chem. 10.1002/ange.201916352

Link to VoR: <http://dx.doi.org/10.1002/anie.201916352>
<http://dx.doi.org/10.1002/ange.201916352>

RESEARCH ARTICLE

Pre-targeted Imaging of Protease Activity Via *In Situ* Assembly of NanoparticlesZixin Chen,[†] Min Chen,[†] Kaixiang Zhou, and Jianghong Rao*

Abstract: Pre-targeted strategies combine high specificity of macromolecules such as antibodies for target binding and rapid clearance of small molecular ligands to image target molecules. However, pre-targeted imaging of the activity of enzymes has not been described likely due to the lack of a mechanism to retain the injected substrate in the first step for subsequent labeling. Here we report the use of two bioorthogonal reactions—the condensation reaction of aromatic nitriles and aminothiols, and the inverse-electron demand Diels-Alder reaction (IEDDA) between tetrazine and trans-cyclooctene (TCO)—to develop a novel strategy for pre-targeted imaging of the activity of proteases. The substrate probe bearing TCO (TCO-C-SNAT4) can be selectively activated by an enzyme target (e.g. caspase-3/7), which triggers macrocyclization and subsequent *in situ* self-assembly into nanoaggregates retained at the target site. Our results show that tetrazine-imaging tag conjugate is able to label TCO in the nanoaggregates to generate selective signal retention for imaging *in vitro*, in cells and in mice. Due to the decoupling of enzyme activation and imaging tag immobilization, TCO-C-SNAT4 can be repetitively injected to generate and accumulate more TCO-nanoaggregates for click labeling. This strategy should be particularly attractive for imaging the activity of enzymes with slow kinetics using short-lived radioisotopes.

Introduction

Pre-targeted imaging uses a targeting vector with a handle for orthogonal coupling and an imaging probe that is introduced later to conjugate with the handle on the targeting vector specifically through a secondary covalent or non-covalent interaction *in vivo*. The targeting vector is administered first and after a waiting period when the targeting vector in blood circulation is cleared out, then the imaging probe is injected. It decouples the target binding molecule from the imaging tag and offers the flexibility to optimize kinetics of both steps independently. For example, in radioimmunodiagnosis or radioimmunotherapy, a radioisotope is delivered to the target site often by conjugating to an antibody for imaging or treatment. This strategy often produces a low tumor-to-blood ratio and use of radioisotopes with long half-lives such as ⁸⁹Zr ($t_{1/2} = 3.3$ days) is necessary since it can take up to several days for antibodies to be cleared out in order to achieve optimal biodistributions.^[1] Long blood circulation time of conjugated antibodies raises concerns on prolonged radiation toxicity to healthy tissues. In pre-targeted imaging, the radioisotope is decoupled from the antibody and conjugated to a small molecule

that can be cleared out quickly, which would allow the use of radioisotopes with relatively short half-lives and thus reduce the duration of systemic exposure to radiation toxicity.^[1d-g] This approach has also been used with nanoparticles for cancer imaging. The nanoparticles bearing click reaction handles were first preferentially retained in tumor through enhanced permeability and retention (EPR) effect, and subsequently labeled through click reaction by a ligand with a radionuclide.^[2] In metabolic labeling, a large fluorophore on the probe may negatively impact the incorporation efficiency. With the pre-targeting approach, a probe with a small click reaction handle is used first for enzymatic incorporation into glycans,^[3] proteins,^[4] DNA^[5] or lipids^[6], followed by click labeling with the imaging tag. In this work, we report the use of pre-targeting approach to image the activity of hydrolytic enzymes.

Proteases are tightly regulated in normal and different disease conditions, and their activity levels can be used to assess some of the underlying biochemical events taking place at disease sites and provide prognostic information for the disease.^[7] We have developed a strategy called target-enabled *in-situ* ligand aggregation (TESLA) for non-invasive imaging of enzyme activity by fluorescence,^[8] positron emission tomography (PET) imaging^[9] and T1-weighted magnetic resonance imaging (MRI).^[10] This platform is empowered by the bioorthogonal condensation reaction between an aromatic nitrile and cysteine.^[11] A TESLA probe is composed of a scaffold containing an aromatic nitrile such as cyanoquinoline^[8-10] or pyrimidinecarbonitrile^[11a] and a masked cysteine that can be activated by enzymatic cleavage. Upon target protease activation, the unmasked cysteine reacts with the aromatic nitrile in a biocompatible fashion to form a macrocyclic product that subsequently proceeds to *in-situ* aggregation promoted by hydrophobic and π - π interactions resulting in enhanced retention at target site.^[11a] Therefore, we hypothesized that the TESLA strategy could be applied to pre-targeted imaging of the activity of proteases (Figure 1). Specifically, a click reaction handle is incorporated into the TESLA probe. This target-specific probe bearing the handle is first activated by the enzyme of interest, followed by cyclization and self-assembly. After sufficient activation by the enzyme to achieve high accumulation of the handle at the target site, the imaging tag will be administered subsequently to label the handle through clicking onto the nanoaggregates at the target site. Using chemotherapy-induced apoptosis in HeLa and H460 tumor cells, we demonstrated this pre-targeted imaging strategy in cells and in living animals for fluorescence and PET imaging of caspase-3/7 activity. Our results have shown that TESLA can be applied to pre-target the enzymatic activity for imaging.

[a] Z. Chen, ^[†] Dr. M. Chen, ^[†] Dr. K. Zhou, Prof. J. Rao
Departments of Radiology and Chemistry, Molecular Imaging
Program at Stanford
Stanford University School of Medicine
Stanford, CA 94305 (USA)
E-mail: jrao@stanford.edu

[†] These authors contributed equally.

Supporting Information for this article is given via a link at the end of the document.

Results and Discussion

RESEARCH ARTICLE

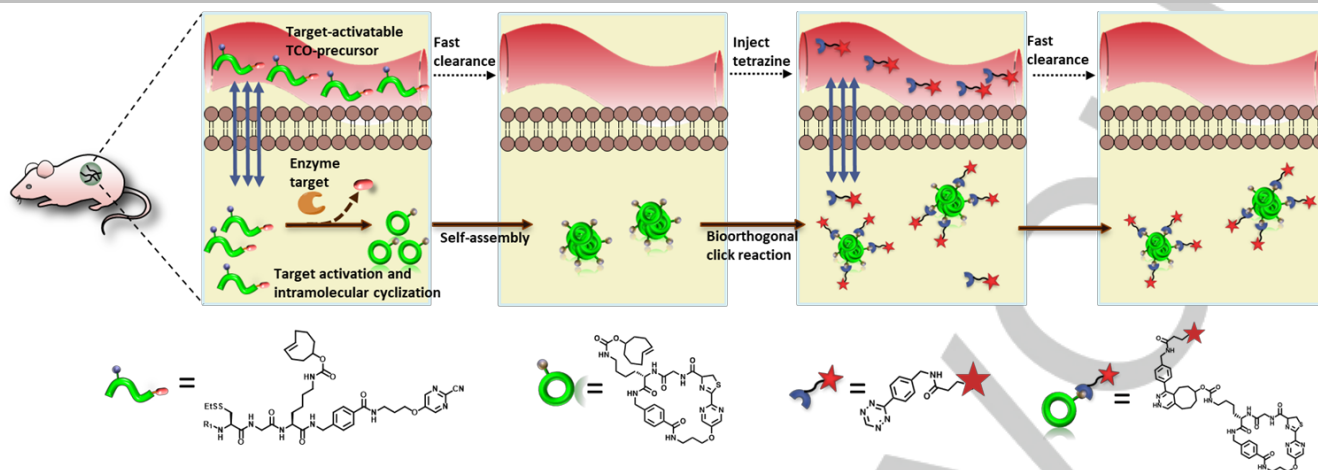


Figure 1. Schematic illustration of pre-targeted imaging of enzyme activity based on target-enabled *in situ* ligand aggregation.

In vitro validation of TCO-C-SNAT4

One of the fastest bioorthogonal reactions is the inverse-electron demand Diels-Alder reaction (IEDDA) between tetrazines (Tz) and trans-cyclooctene (TCO), which was first described by Fox and coworkers in 2008^[12] and later demonstrated by other groups for pre-targeted imaging.^[13] We thus used the TCO and Tz pair for the second step labeling of assembled nanoaggregates (Figure 1). We first designed and synthesized TCO-C-SNAT4 that can be specifically activated by active caspases-3/7, the downstream effectors in the apoptosis cascade. TCO-C-SNAT4 uses tetrapeptide Asp-Glu-Val-Asp (DEVD) as its caging group, which can be cleaved by active caspase-3/7 (Figure 2a). Details of synthesis of this probe are described in Supporting Information.

Enzymatic activation of TCO-C-SNAT4 was tested by adding human recombinant caspase-3 enzyme (2×10^{-3} U mL⁻¹) to a solution of TCO-C-SNAT4 (20 μ M) in caspase buffer. After overnight incubation at 37 °C, aliquots of the reaction solution were analyzed by high-performance liquid chromatography (HPLC) (Figure 2b) and mass spectrometry (Figure S1). A new HPLC peak close to TCO-C-SNAT4 was revealed by mass spectrometry to be cycl-TCO-SNAT4. Another small peak close to the major product cycl-TCO-SNAT4 gave the same molecular weight as TCO-C-SNAT4 but did not react with tetrazine, suggesting it probably be the inactive *cis*-cyclooctene isomer. The formation of the nano-aggregates of cycl-TCO-SNAT4 was confirmed by dynamic light scattering (DLS) and transmission electron microscopy (TEM) with a size distribution between 100-400 nm (Figure 2c,e). This result confirms that TCO-C-SNAT4 can be activated by caspase-3 enzyme followed by macrocyclization and aggregation to form nanoaggregates, which was similar to what we have observed with other TESLA probes.

To test if tetrazine was able to undergo fast IEDDA reaction with nanoaggregates, the solution mixture of TCO-C-SNAT4 and caspase-3 enzyme was then treated with Tz-BDP (20 μ M). Coupling reaction completed in 30 min at room temperature, as confirmed by HPLC (Figure 2b). In addition to forming cycl-SNAT4-BDP, a side product, its dihydropyridazine isomer was also detected by mass spectrometry (Figure 2b and Figure S1). Complete conversion of TCO in the nanoaggregates was a surprising observation since some TCO could be packed inside the nanoaggregates. A likely explanation is that the packing of the nanoaggregates is loose and dynamic considering that the nanoaggregates formed through non-covalent interactions. There may be a dynamic exchange between nonaggregated and aggregated forms of cycl-TCO-SNAT4. This notion is further supported by the reaction kinetics measurement.

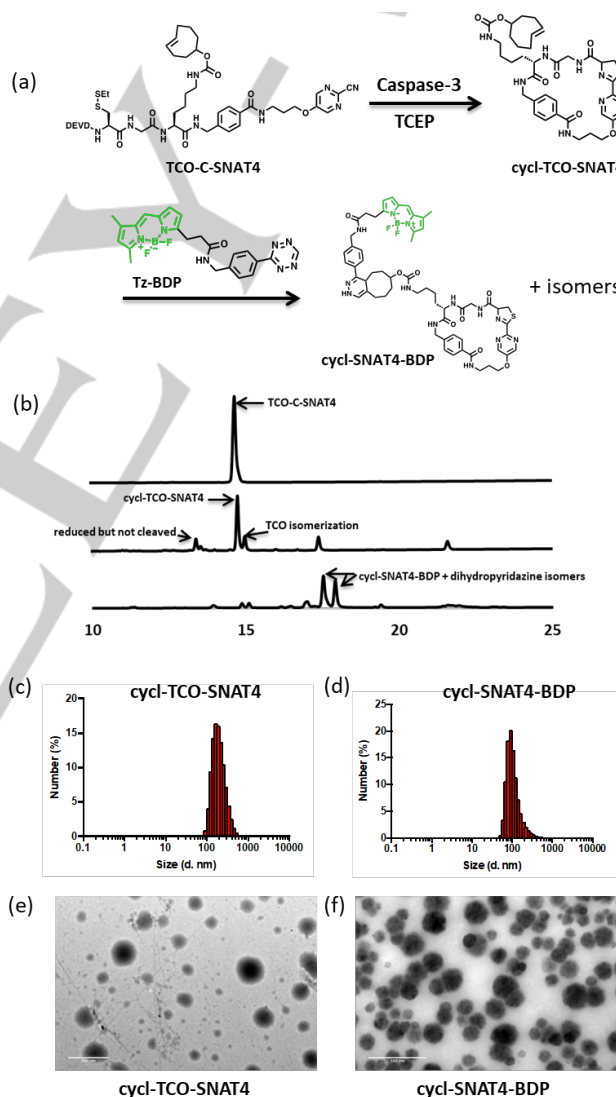


Figure 2. (a) Schematic illustration of activation of TCO-C-SNAT4 by caspase-3 followed by IEDDA reaction with Tz-BDP. (b) HPLC traces of TCO-C-SNAT4 (upper), after incubation with caspase-3 (2×10^{-3} U mL⁻¹) at 37 °C in caspase-3 buffer overnight (middle) and after addition of Tz-BDP (bottom). Scale bar: 500 nm. (c-d) DLS analysis of particle sizes of (c) cycl-TCO-SNAT4 and (d) cycl-SNAT4-BDP. (e-f) TEM images of particles of (e) cycl-TCO-SNAT4 and (f) cycl-SNAT4-BDP.

RESEARCH ARTICLE

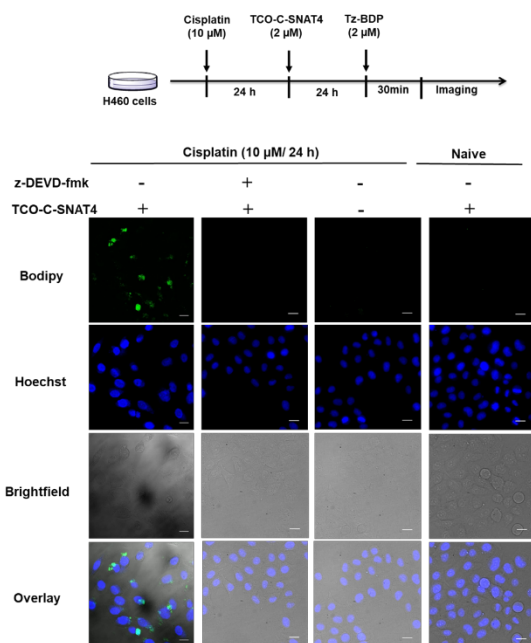


Figure 3. H460 cells were treated with cisplatin (10 μM) for 24 hours to induce apoptosis before incubation with z-VAD-fmk (0 or 50 μM) for 1 hour. Cells were then incubated with TCO-C-SNAT4 (2 μM) for 24 hours and then with Tz-BDP (2 μM) for 30 minutes. Scale bar: 20 μm .

We measured the reaction rate of free TCO-C-SNAT4 and cycl-TCO-SNAT4 nanoaggregates with Tz-BDP. Upon reaction with TCO, the quenching effect of tetrazine is lost and the fluorescence of BODIPY is restored.^[14] Thus the change of the fluorescence of Tz-BDP at 510 nm during the reaction can be used to extrapolate the reaction rate (Supporting Information, Figure S2). The second-order rate constant of TCO-C-SNAT4 with Tz-BDP was estimated to be $380 \pm 20 \text{ M}^{-1}\text{s}^{-1}$, which was consistent with previously reported rates.^[12] In comparison, the value for cycl-TCO-SNAT4 nanoaggregates was just slightly smaller ($294 \pm 48 \text{ M}^{-1}\text{s}^{-1}$). This result may also reflect the dynamic exchange between aggregated and nonaggregated cycl-TCO-SNAT4. The product cycl-SNAT4-BDP interacted and formed nanoaggregates. Interestingly they had a slightly smaller size distribution between 60–300 nm than that of cycl-TCO-SNAT4, as shown by DLS and TEM (Figures 2d,f).

Imaging caspase-3/7 activity in cisplatin-treated H460 cells and in STS-treated HeLa cells using TCO-C-SNAT4

Pre-targeted imaging of enzyme activity with TCO-C-SNAT4 was investigated through imaging drug-induced apoptosis in both cisplatin-treated human non-small cell lung cancer cell H460 (Figure 3) and in STS-treated HeLa cells (Supporting Information, Figure S3). At 10 μM cisplatin treatment induced apoptosis in a subset of H460 cells and STS treatment induces apoptosis in almost all HeLa cells. After drug treatments, cells were incubated with TCO-C-SNAT4 for 24 hours followed by addition of Tz-BDP. In both models, extensive fluorescence accumulation was observed in drug-induced apoptotic cells, and only negligible fluorescence in untreated viable cells, indicating non-specific binding of Tz-BDP is minimal. As expected, treatment of caspase-3 inhibitor z-VAD-fmk rendered negligible fluorescence retention, confirming the activation of TCO-C-SNAT4 by the effective caspases in cisplatin-treated H460 cells. When we premixed TCO-C-SNAT4 with tetrazine ethylamine to block click reaction with Tz-BDP, we observed no fluorescence signal in STS-treated HeLa cells, confirming fluorescence retention was achieved through the click reaction between cycl-SNAT4-BDP and Tz-BDP. The kinetics of the IEDDA reaction between cycl-TCO-SNAT4 and Tz-BDP in cells was also investigated in STS-treated H460 cells by monitoring fluorescence change in real time immediately after Tz-BDP was added (Supporting Information, Movie S1). Fluorescent intensity plateaued in as short as 10 minutes, suggesting fast IEDDA reaction between cycl-TCO-SNAT4 and Tz-BDP in cells. We also measured the cellular toxicity of TCO-C-SNAT4 and Tz-BDP in H460 cells, and neither compound was found to show significant toxicity up to 100 μM (Supporting Information, Figure S4).

Probing IEDDA reaction efficiency in labeling nanoaggregates in vivo

We next investigated if cycl-TCO-SNAT4 nanoaggregates by Tz-BDP could be labeled by the IEDDA labeling reaction in vivo. A series of concentration of cycl-TCO-SNAT4 nanoaggregates (0.1, 1, 10, 50, 100 and 500 μM) was prepared and DLS measurement showed the dependence of the size of nanoaggregates on the concentration of cycl-TCO-SNAT4 (Supporting Information, Figure S5). The solutions of cycl-TCO-SNAT4 remained homogeneous up to 100 μM in PBS buffer and a significant amount of precipitate was observed when the concentration was 500 μM or more. We injected these nanoaggregate solutions subcutaneously into the mice, followed by immediate i.v. injection of Tz-Cy5 (Supporting Information, Figure S5). Fluorescence imaging revealed that the fluorescence intensity at the injection sites depended on the concentration of

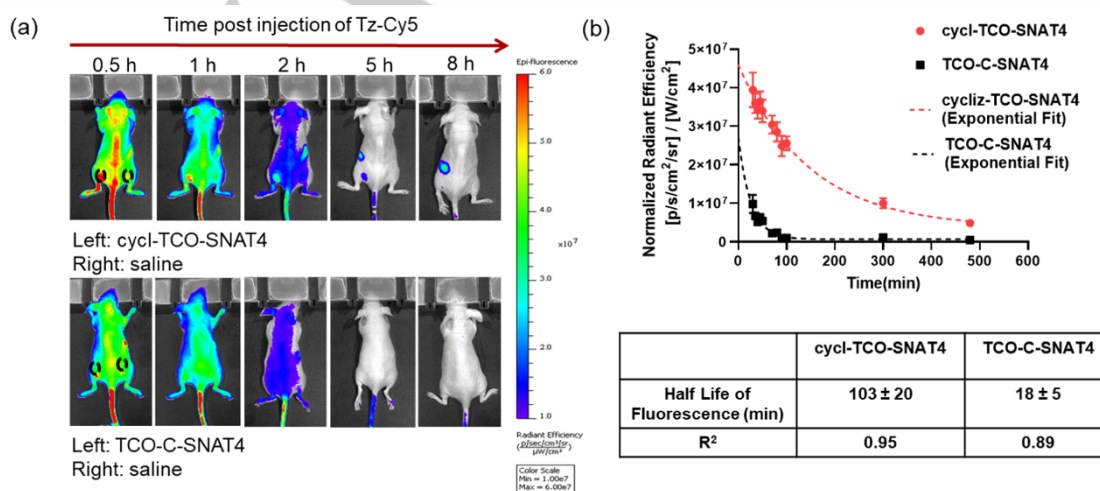


Figure 4. (a) Mice were injected subcutaneously with 5 nmol of cycl-TCO-SNAT4 or TCO-C-SNAT4 on the left thigh and saline on the right thigh followed by immediate i.v. injection of Tz-Cy5 (5 nmol) and imaged for 8 hours. (b) Decay of fluorescence signal at the injection sites of cycl-TCO-SNAT4 and TCO-C-SNAT4 over 8 hours. ($n = 3$) ****, $P < 0.001$.

RESEARCH ARTICLE

the nanoaggregates. However, the highest fluorescence intensity came from the site injected with 100 μM solution instead of 500 μM . This observation is probably due to the formation of insoluble aggregates at this high concentration (as observed *in vitro*) resulting some of TCOs inaccessible to tetrazine.

On the other hand, controls with non-aggregate small molecule TCO-C-SNAT4, cycl-TCO-SNAT4 premixed with tetrazine ethylamine, and saline were also injected subcutaneously. These control sites showed much lower fluorescence intensity than the site injected with cycl-TCO-SNAT4 nanoparticles (Supporting Information, Figure S6), indicating that TZ-Cy5 reacted with pre-formed nanoparticles and was better retained at the nanoparticle injection site.

The *in vivo* half-life of pre-formed nanoaggregates was further estimated by fluorescence imaging. Pre-formed cycl-TCO-SNAT4 nanoparticles at 100 μM were subcutaneously injected at the left thigh of a mouse, followed by immediate *i.v.* injection of Tz-Cy5 (Figure 4). Saline was injected contralaterally as the background control for the normalization of fluorescent signal. After subtracting the background signal and fitting the result with an exponential decay curve, the half-life for the fluorescent signals was calculated to be about 103 minutes for cycl-TCO-SNAT4 nanoparticles. Similarly, we estimated the *in vivo* half-life for TCO-C-SNAT4 to be about 18 minutes (Figure 4d). The difference in the fluorescence decay between the two substrates reflects their different diffusion rate. The observed fluorescence retention and decay of the pre-formed nanoparticle also reflects the dynamic processes of nanoparticle retention, disassembly and diffusion since the nanoaggregates are associated through non-covalent interactions.

Pre-targeted fluorescence imaging of caspase-3/7 activity *in vivo*

After having demonstrated the *in vivo* labeling of pre-formed nanoaggregates by tetrazine, we next tested it for pre-targeted imaging of caspase-3/7 activity in drug-treated tumor xenografts in live animals. Mice bearing H460 tumor were first treated with cisplatin (10 μM , *i.t.*), and 24-hour later, TCO-C-SNAT4 (10 nmol) was injected intravenously, followed by intravenous injection of Tz-Cy5 (5 nmol) after 30 minutes. Fluorescence at tumor sites

was monitored for up to 2 hours (Figure 5). Significant retention of fluorescent signal in the cisplatin-treated mouse group was observed in as short as 5 minutes and lasted for 100 minutes while only negligible signal retention was observed for the untreated group. In control groups, only negligible fluorescence retention was observed at tumor sites mice injected with saline only, or when TCO-C-SNAT4 was premixed with tetrazine-ethylamine before injected into mice or when the mice were treated with caspase inhibitor z-VAD-fmk (Supporting Information, Figure S7). These results support that the aggregated particles formed by caspase-3/7 activity in apoptotic tumors can be labeled by tetrazine through the IEDDA reaction as well and are retained for a prolonged period of time to enhance imaging contrast.

Different from proteins and antibodies whose levels remain relatively stable during the pre-targeted imaging, the enzymatic activity may be exploited to generate more nanoaggregates to enrich the target abundance for subsequent labeling. To demonstrate this feature, we injected treated animals with TCO-C-SNAT4 (*i.v.*, 10 nmol) 3 times (every hour) prior to the injection of Tz-Cy5 (5 nmol), followed by fluorescence imaging for 2 hours (Supporting Information, Figure S8). The one-hour interval between consecutive TCO-C-SNAT injection was chosen based on the rapid clearance of consecutive TCO-C-SNAT from circulation. In comparison to the control groups receiving no or single injection of TCO-C-SNAT, the retention of Cy5 fluorescent signal in tumors in the 3x injection group was significantly higher, which was further confirmed by the histological analysis of the excised tumor tissue sections (Supporting Information, Figure S9). This result demonstrates the advantage of combining the pre-targeted imaging approach with TESLA probes in imaging the enzyme activity.

Pre-targeted positron emission tomography (PET) imaging of caspase-3/7 activity *in vivo*

We next investigated the retention of the nanoaggregates using more quantitative PET imaging to demonstrate the applicability of the method for other imaging modalities. To estimate the half-life of nanoaggregates *in vivo*, we chose ^{64}Cu a PET isotope with a longer radioactivity half-life (12.7 hours) than ^{18}F (109.7 mins). To mice bearing H460 tumors that were treated with cisplatin were

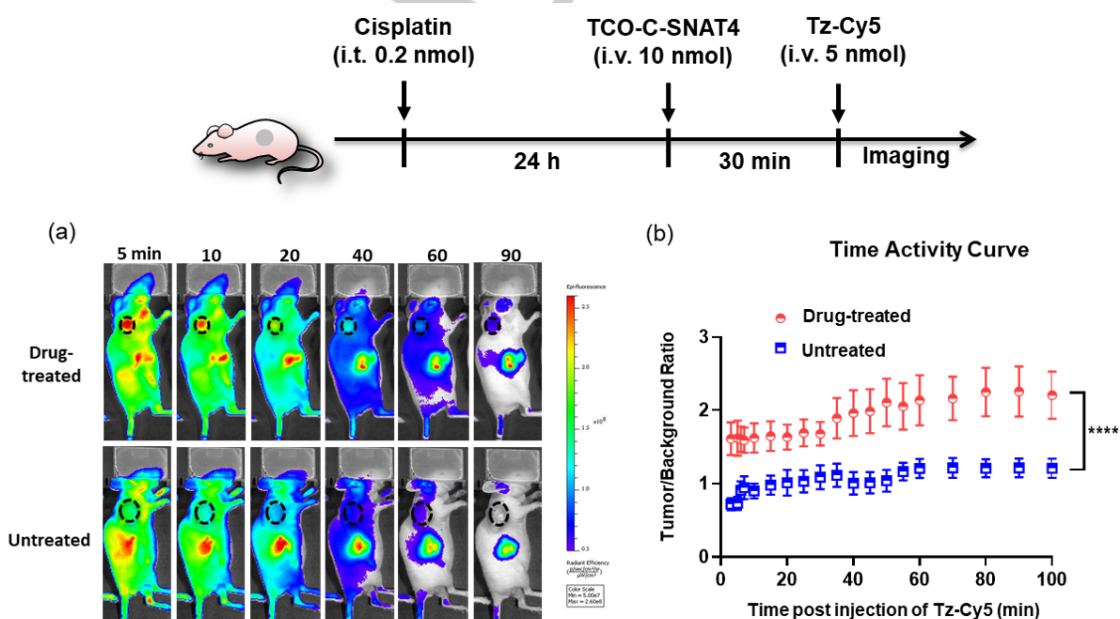


Figure 5. (a) Mice bearing H460 tumors were first treated with cisplatin for 24 hours before injected with TCO-C-SNAT4 (10 nmol). After 30 minutes mice were injected Tz-Cy5 (5 nmol) and imaged in real-time. Tumors are highlighted in black circles. (b) Quantification of fluorescent signal in tumors. ($n = 3$) ****, $P < 0.001$.

RESEARCH ARTICLE

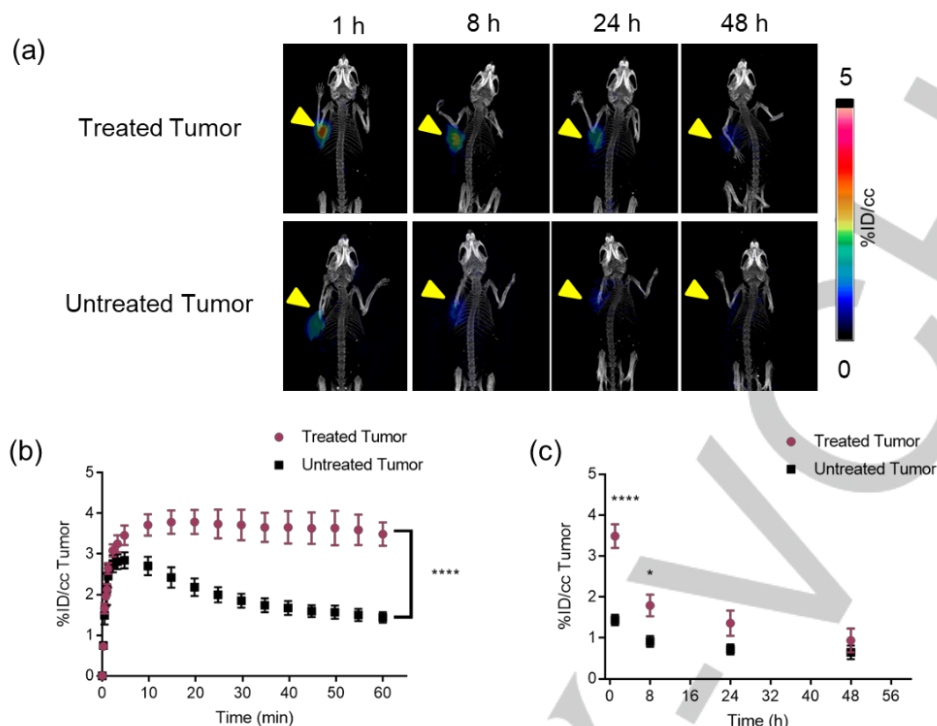


Figure 6. (a) PET/CT imaging of nude mice with cisplatin-treated H460 tumor (left) and untreated H460 tumor (right) at 1, 8, 24, and 48 h. Mice intratumorally received TCO-C-SNAT4 (5 nmol in 100 μ l volume) followed by i.v. injection of Tz-DOTA- 64 Cu (\sim 400 μ Ci). A threshold method was utilized to mask the relatively high uptake in liver, spleen, kidney and bladder. Sectional images without thresholding analysis are presented in Supporting Information Figure S12. (b) Time-activity curve of PET signal at tumor site from 0 to 60 minutes. (c) Quantification of radioactivity accumulated in the tumors at 1, 8, 24 and 48 hours after Tz-DOTA- 64 Cu injection. Tumors were indicated with white circles. (n = 4) *, P < 0.05; ****, P < 0.001.

injected TCO-C-SNAT4 (5 nmol, i.t.) followed by injecting 64 Cu-chelated Tz-DOTA (\sim 400 μ Ci) for PET/CT imaging (Figure 6). A 2.5-fold difference was observed between treated ($3.5\% \pm 0.3$ ID/cc) and untreated group ($1.4\% \pm 0.1\%$ ID/cc) after 1 hour and significant differences can be identified in as short as 10 minutes postinjection of the radiolabeled tetrazine (Figure 6b). Mice were monitored for two days and radioactivity signal retention was quantified through PET/CT. Mice receiving cisplatin treatment showed initial signal retention at the tumor site followed by slow signal decay ($t_{1/2} = 244$ minutes) while the untreated mice showed a steep signal decay curve following initial uptake ($t_{1/2} = 37$ minutes) (Figure 6; Supporting Information, Figure S10). Biodistribution analysis at 1 hour showed renal clearance was the major clearance pathway, and at 48 hours significant amounts of radioactivity were still retained in GI tract and liver (Supporting Information, Figure S11). The pharmacokinetics of the tetrazine-radiionuclide conjugate may be improved by modulating hydrophilicity, charges and chelator structure as previously reported.^[13b, 13f] Similar to previous report on the stability of TCO^[15], we also observed isomerization of TCO in neat solution over several days which was accelerated after repeating freeze-thawing of the stock solution. Thus TCO-C-SNAT4 was always freshly prepared for each animal experiment to maintain high purity of the probe. We also tested the stability of TCO-C-SNAT4 in mouse serum. HPLC and mass spectrometry analysis showed a clean conversion of trans-cyclooctene-C-SNAT4 to cis-cyclooctene-C-SNAT4 with a half-life of around 4 hours (Supporting Information, Figure S13). This isomerization is likely caused by copper-containing proteins in serum and can potentially be optimized through increasing steric hindrance as previously reported.^[13h]

Conclusion

In this work, we have developed a novel strategy to expand pre-targeted imaging to the activity of proteases based on our TESLA platform. This approach uses two bioorthogonal reactions—the condensation reaction of aromatic nitriles and aminothiols, and the inverse-electron demand Diels-Alder reaction (IEDDA) between tetrazines and trans-cyclooctene: the first to generate in situ assembled nanoparticles upon the target protease activation, and the second to in vivo label assembled nanoparticles. We have demonstrated it using apoptotic enzyme caspas-3/7 as the model target in mice across two imaging modalities—fluorescence and positron emission tomography. With the decoupling of enzyme activation from immobilization of imaging tag, optimal kinetics and dose may be obtained for maximal imaging contrast even with short-lived radioisotopes. This approach should be readily adapted for others enzyme targets (by modifying the substrate) and even targeted drug delivery through the IEDDA reaction triggered release.^[16]

Acknowledgements

This work was supported by a grant from the National Cancer Institute (NCI) Stanford CCNE-TD (U54CA199075). M. C. acknowledged the support by the Stanford Cancer Translational

RESEARCH ARTICLE

Nanotechnology Training grant (T32CA196585) funded by the NCI.

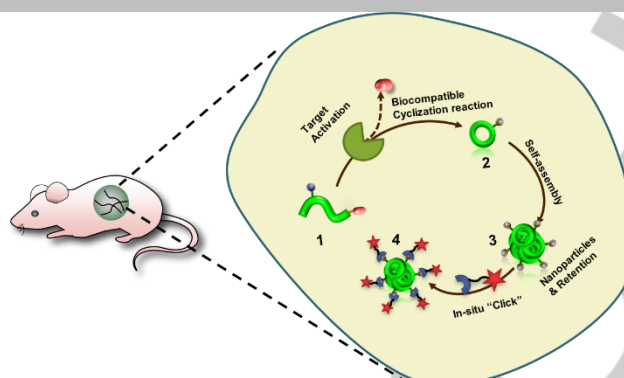
Keywords: self-assembly nanoparticle • pre-targeted imaging • bioorthogonal reaction • in vivo imaging • caspase

- [1] a) N. K. Devaraj, R. Weissleder, *Acc. Chem. Res.* **2011**, *44*, 816-827; b) J. C. Maza, J. R. McKenna, B. K. Raliski, M. T. Freedman, D. D. Young, *Bioconjugate Chem.* **2015**, *26*, 1884-1889; c) C. J. Pickens, S. N. Johnson, M. M. Pressnall, M. A. Leon, C. J. Berkland, *Bioconjugate Chem.* **2018**, *29*, 686-701; d) M. Altai, R. Membreno, B. Cook, V. Tolmachev, B. M. Zeglis, *J. Nucl. Med.* **2017**, *58*, 1553-1559; e) M. Patra, K. Zarschler, H. J. Pietzsch, H. Stephan, G. Gasser, *Chem. Soc. Rev.* **2016**, *45*, 6415-6431; f) R. M. Sharkey, *Clin. Cancer Res.* **2005**, *11*, 7109s-7121s; g) O. C. Boerman, F. G. van Schaijk, W. J. Oyen, F. H. Corstens, *J. Nucl. Med.* **2003**, *44*, 400-411; h) T. K. Nayak, M. W. Brechbiel, *Bioconjugate Chem.* **2009**, *20*, 825-841; i) S. M. Larson, J. A. Carrasquillo, N. K. Cheung, O. W. Press, *Nat. Rev. Cancer* **2015**, *15*, 347-360.
- [2] a) S. B. Lee, H. L. Kim, H. J. Jeong, S. T. Lim, M. H. Sohn, D. W. Kim, *Angew. Chem. Int. Ed. Engl.* **2013**, *52*, 10549-10552; b) S. Hou, J. S. Choi, M. A. Garcia, Y. Xing, K. J. Chen, Y. M. Chen, Z. K. Jiang, T. Ro, L. Wu, D. B. Stout, J. S. Tomlinson, H. Wang, K. Chen, H. R. Tseng, W. Y. Lin, *ACS Nano* **2016**, *10*, 1417-1424; c) C. Denk, D. Svatunek, S. Mairinger, J. Stanek, T. Filip, D. Matscheko, C. Kuntner, T. Wanek, H. Mikula, *Bioconjugate Chem.* **2016**, *27*, 1707-1712; d) O. Keinänen, E. M. Mäkilä, R. Lindgren, H. Virtanen, H. Liljenbäck, V. Oikonen, M. Sarparanta, C. Molthoff, A. D. Windhorst, A. Roivainen, J. J. Salonen, A. J. Airaksinen, *ACS Omega* **2017**, *2*, 62-69.
- [3] a) P. V. Chang, J. A. Prescher, E. M. Sletten, J. M. Baskin, I. A. Miller, N. J. Agard, A. Lo, C. R. Bertozzi, *Proc. Natl. Acad. Sci. U. S. A.* **2010**, *107*, 1821-1826; b) V. V. Fokin, *ACS Chem. Biol.* **2007**, *2*, 775-778; c) T. L. Hsu, S. R. Hanson, K. Kishikawa, S. K. Wang, M. Sawa, C. H. Wong, *Proc. Natl. Acad. Sci. U. S. A.* **2007**, *104*, 2614-2619; d) S. T. Laughlin, J. M. Baskin, S. L. Amacher, C. R. Bertozzi, *Science* **2008**, *320*, 664-667; e) J. A. Prescher, C. R. Bertozzi, *Nat. Chem. Biol.* **2005**, *1*, 13-21; f) D. Rabuka, S. C. Hubbard, S. T. Laughlin, S. P. Argade, C. R. Bertozzi, *J. Am. Chem. Soc.* **2006**, *128*, 12078-12079.
- [4] a) K. E. Beatty, J. C. Liu, F. Xie, D. C. Dieterich, E. M. Schuman, Q. Wang, D. A. Tirrell, *Angew. Chem. Int. Ed. Engl.* **2006**, *45*, 7364-7367; b) A. E. Speers, B. F. Cravatt, *Chem. Bio.* **2004**, *11*, 535-546.
- [5] a) A. Salic, T. J. Mitchison, *Proc. Natl. Acad. Sci. U. S. A.* **2008**, *105*, 2415-2420; b) C. Y. Jao, A. Salic, *Proc. Natl. Acad. Sci. U. S. A.* **2008**, *105*, 15779-15784.
- [6] a) A. B. Neef, C. Schultz, *Angew. Chem. Int. Ed. Engl.* **2009**, *48*, 1498-1500; b) A. Laguerre, C. Schultz, *Curr. Opin. Cell Biol.* **2018**, *53*, 97-104.
- [7] a) C. Lopez-Otin, J. S. Bond, *J. Biol. Chem.* **2008**, *283*, 30433-30437; b) C. Lopez-Otin, L. M. Matrisian, *Nat. Rev. Cancer* **2007**, *7*, 800-808; c) B. Turk, *Nat. Rev. Drug Discov.* **2006**, *5*, 785-799; d) M. Merdanovic, T. Monig, M. Ehrmann, M. Kaiser, *ACS Chem. Biol.* **2013**, *8*, 19-26.
- [8] a) G. Liang, H. Ren, J. Rao, *Nat. Chem.* **2010**, *2*, 54-60; b) D. Ye, G. Liang, M. L. Ma, J. Rao, *Angew. Chem. Int. Ed. Engl.* **2011**, *50*, 2275-2279; c) D. Ye, A. J. Shuhendler, L. Cui, L. Tong, S. S. Tee, G. Tikhomirov, D. W. Felsher, J. Rao, *Nat. Chem.* **2014**, *6*, 519-526.
- [9] a) B. Shen, J. Jeon, M. Palner, D. Ye, A. Shuhendler, F. T. Chin, J. Rao, *Angew. Chem. Int. Ed. Engl.* **2013**, *52*, 10511-10514; b) M. Palner, B. Shen, J. Jeon, J. Lin, F. T. Chin, J. Rao, *J. Nucl. Med.* **2015**, *56*, 1415-1421; c) T. H. Witney, A. Hoehne, R. E. Reeves, O. Ilovich, M. Namavari, B. Shen, F. T. Chin, J. Rao, S. S. Gambhir, *Clin. Cancer Res.* **2015**, *21*, 3896-3905.
- [10] a) G. Liang, J. Ronald, Y. Chen, D. Ye, P. Pandit, M. L. Ma, B. Rutt, J. Rao, *Angew. Chem. Int. Ed. Engl.* **2011**, *50*, 6283-6286; b) D. Ye, P. Pandit, P. Kempen, J. Lin, L. Xiong, R. Sinclair, B. Rutt, J. Rao, *Bioconjugate Chem.* **2014**, *25*, 1526-1536; c) D. Ye, A. J. Shuhendler, P. Pandit, K. D. Brewer, S. S. Tee, L. Cui, G. Tikhomirov, B. Rutt, J. Rao, *Chem. Sci.* **2014**, *4*, 3845-3852; d) A. J. Shuhendler, D. Ye, K. D. Brewer, M. Bazalova-Carter, K. H. Lee, P. Kempen, K. Dane Wittrup, E. E. Graves, B. Rutt, J. Rao, *Sci. Rep.* **2015**, *5*, 14759.
- [11] a) Z. Chen, M. Chen, Y. Cheng, T. Kowada, J. Xie, X. Zheng, J. Rao, *Angew. Chem. Int. Ed. Engl.* **2020**, *59*, 3272-3279; b) H. Ren, F. Xiao, K. Zhan, Y. P. Kim, H. Xie, Z. Xia, J. Rao, *Angew. Chem. Int. Ed. Engl.* **2009**, *48*, 9658-9662.
- [12] M. L. Blackman, M. Royzen, J. M. Fox, *J. Am. Chem. Soc.* **2008**, *130*, 13518-13519.
- [13] a) Z. Li, H. Cai, M. Hassink, M. L. Blackman, R. C. Brown, P. S. Conti, J. M. Fox, *Chem. Comm.* **2010**, *46*, 8043-8045; b) J. P. Meyer, P. Kozlowski, J. Jackson, K. M. Cunanan, P. Adumeau, T. R. Dilling, B. M. Zeglis, J. S. Lewis, *J. Med. Chem.* **2017**; c) R. Rossin, T. Lappchen, S. M. van den Bosch, R. Laforest, M. S. Robillard, *J. Nucl. Med.* **2013**, *54*, 1989-1995; d) R. Rossin, P. R. Verkerk, S. M. van den Bosch, R. C. Vuldgers, I. Verel, J. Lub, M. S. Robillard, *Angew. Chem. Int. Ed. Engl.* **2010**, *49*, 3375-3378; e) R. Selvaraj, B. Giglio, S. Liu, H. Wang, M. Wang, H. Yuan, S. R. Chintala, L. P. Yap, P. S. Conti, J. M. Fox, Z. Li, *Bioconjugate Chem.* **2015**, *26*, 435-442; f) B. M. Zeglis, C. Brand, D. Abdel-Atti, K. E. Carnazza, B. E. Cook, S. Carlin, T. Reiner, J. S. Lewis, *Mol. Pharm.* **2015**, *12*, 3575-3587; g) B. M. Zeglis, K. K. Sevak, T. Reiner, P. Mohindra, S. D. Carlin, P. Zanzonico, R. Weissleder, J. S. Lewis, *J. Nucl. Med.* **2013**, *54*, 1389-1396; h) R. Rossin, S. M. van den Bosch, W. Ten Hoeve, M. Carvelli, R. M. Versteegen, J. Lub, M. S. Robillard, *Bioconjugate Chem.* **2013**, *24*, 1210-1217.
- [14] N. K. Devaraj, S. Hilderbrand, R. Upadhyay, R. Mazitschek, R. Weissleder, *Angew. Chem. Int. Ed. Engl.* **2010**, *49*, 2869-2872.
- [15] H. E. Murrey, J. C. Judkins, C. W. am Ende, T. E. Ballard, Y. Fang, K. Riccardi, L. Di, E. R. Guilmette, J. W. Schwartz, J. M. Fox, D. S. Johnson, *J. Am. Chem. Soc.* **2015**, *137*, 11461-11475.
- [16] a) R. Rossin, R. M. Versteegen, J. Wu, A. Khasanov, H. J. Wessels, E. J. Steenbergen, W. Ten Hoeve, H. M. Janssen, A. van Onzen, P. J. Hudson, M. S. Robillard, *Nat. Comm.* **2018**, *9*, 1484; b) Y. Zheng, X. Ji, B. Yu, K. Ji, D. Gallo, E. Csizmadia, M. Zhu, M. R. Choudhury, L. K. C. De La Cruz, V. Chittavong, Z. Pan, Z. Yuan, L. E. Otterbein, B. Wang, *Nat. Chem.* **2018**, *10*, 787-794.

RESEARCH ARTICLE

RESEARCH ARTICLE

Double click imaging: A pre-targeting approach for imaging enzyme activity in vivo based on target-enabled in situ ligand aggregation (TESLA). The small molecule is first activated by target enzyme to trigger macrocyclization and nanoaggregation in cells, followed by bioorthogonal click labeling with a fluorescent dye or radionuclide to generate imaging contrast.



Zixin Chen,[†] Min Chen,[†] Kaixiang Zhou, and Jianghong Rao*

Page No. – Page No.

Pre-targeted imaging of protease activity via in situ assembly of nanoparticles

Accepted Manuscript